IL NUOVO CIMENTO Vol. 31 C, N. 4 Luglio-Agosto 2008
DOI 10.1393/ncc/i2009-10320-1

# Direct radiative effects by anthropogenic particles at a polluted site: Rome (Italy)

A. Bergamo, F. De Tomasi and M. R. Perrone

*CNISM, Dipartimento di Fisica, Università del Salento - Lecce, Italy*

(ricevuto il 7 Gennaio 2009; approvato il 24 Febbraio 2009; pubblicato online il 20 Marzo 2009)

**Summary.** — The direct radiative effect (DRE) by all (anthropogenic plus natural) and anthropogenic aerosols is calculated at the solar (0.3–4 $\mu$m) and infrared (4–200 $\mu$m) spectral range to better address the annual cycle of the anthropogenic aerosol impact at a site (Rome, Italy) significantly affected by pollution. Aerosol optical and microphysical properties from 2003 AERONET Sun/sky-photometer measurements and solar surface albedos based on MODIS satellite sensor data constitute the necessary input to radiative transfer simulations. Clear- and all-sky conditions are investigated by adopting ISCCP monthly products for high-, mid-, and low-cloud cover. It is shown that monthly mean values of aerosol optical depths by anthropogenic particles ($AOD_a$) are on average more than 50% of the corresponding all-aerosol-optical-depth (AOD) monthly means. In particular, the $AOD_a$/AOD ratio that varies within the (0.51–0.83) on autumn-winter (AW, October-March), varies within the (0.50–0.71) range on spring-summer (SS, April-September) as a consequence of the larger contribution of natural particles on SS. The surface (sfc), all-sky DRE by anthropogenic particles that is negative all year round at solar wavelengths, represents on average 60% and 51% of the all-sky sfc-DRE by all aerosols on AW and SS, respectively. The all-sky atmospheric forcing by anthropogenic particles ($AF_a$) that is positive all year round, is little dependent on seasons: it varies within the (1.0–4.1) $W/m^2$ and (2.0–4.2) $W/m^2$ range on AW and SS, respectively. Conversely, the all-sky AF by all aerosols is characterized by a marked seasonality. As a consequence, the atmospheric forcing by anthropogenic particles that on average is 50% of the AF value on AW, decreases down to 36% of the AF value on SS. Infrared aerosol DREs that are positive all year round are significantly smaller than the corresponding absolute values of solar DREs. Clouds decrease on average ToA- and sfc-DRE absolute values by anthropogenic particles of 36% and 23%, respectively and are quite responsible of the seasonal dependence of aerosol forcing efficiencies by all and anthropogenic aerosols.

PACS 92.60.Mt – Particles and aerosols.
PACS 92.60.Vb – Radiative processes, solar radiation.
PACS 92.70.Cp – Atmosphere.
PACS 92.70.Bc – Land/atmosphere interactions.

## 1. – Introduction

Atmospheric particles of natural and anthropogenic origin influence the Earth's radiation balance and climate mainly in two ways: a) by scattering and absorbing the solar radiation, a phenomenon termed as "aerosol direct radiative effect (DRE)", and b) by acting as cloud condensation nuclei and, thereby, affecting cloud lifetime and properties, a phenomenon termed as "aerosol indirect radiative effect". The assessment of the direct radiative effect by anthropogenic aerosols is of great interest being its level of scientific understanding "medium-low" in accordance with IPCC, 2007 [1]. The high aerosol variability in space and time and the assumptions on aerosol properties are partially responsible for this last result. Quantifying and reducing the uncertainty in aerosol influences on climate is critical to understanding climate change over the industrial period and to improving predictions of future climate change [2]. The Mediterranean basin has a particular relevance in this kind of studies as this area is particularly affected by air pollution. In addition to sea-spray aerosols and mineral dust particles from North Africa, long-range transported urban/industrial and biomass burning aerosols from Northern and Eastern Europe regions converge in the Mediterranean. As a consequence, several studies have indicated that the aerosol radiative forcing is among the highest in the world over the Mediterranean [3, 4]. The seasonal dependence of the DRE by anthropogenic particles ($DRE_a$) at Mediterranean land sites differently affected by anthropogenic pollution has recently been investigated by the authors of this paper [5]. In particular, monthly evolutions of the anthropogenic aerosol impact on the solar and IR direct radiative forcing under all-sky conditions have been analyzed for six different sites: Ispra, Venice, Oristano, Lecce, Lampedusa, and Crete. To this end, aerosol optical and microphysical properties of AERONET Sun/sky photometer data [6] of the year 2003 (the warmest in recent years) have been applied in a radiative transfer code to simulate $DRE_a$ monthly mean values. The use of observation-based aerosol properties is of peculiar importance to reduce uncertainties of model-based results. The AERONET aerosol property's analysis has revealed that Ispra and Venice that were the site with on average larger aerosol loads all year round, also were the sites more affected by anthropogenic particles. In contrast, Lampedusa and Crete were the sites less affected by anthropogenic particles and also characterized by smaller aerosol optical depth (AOD) values. The mean percentage of the $AOD_a$/AOD ratio that was larger than 70% at Ispra and Venice was equal to 40% at Lampedusa and Crete, where $AOD_a$ represents the aerosol optical depth due to anthropogenic particles. A marked seasonality of the aerosol properties dependent on site location has also been observed at all sites. Calculated monthly means of the solar $DRE_a$ at the surface (sfc) and at the top of the atmosphere (ToA) were negative all year round and were also characterized by larger negative values on SS at all sites with the exception of Ispra. Then, it has been shown that anthropogenic particles produce over the central Mediterranean a significant cooling effect both at the surface and at the ToA, and that the cooling effect at the surface is larger than that associated to the ToA. sfc-$DRE_a$ values were up to 7 times larger than ToA-$DRE_a$ values at Ispra. In contrast, mean sfc-$DRE_a$ values were 1.3 times larger than the ToA-$DRE_a$ values at Lampedusa and Crete. However, the differences between averaged values of different sites were smaller than the associated standard deviation. These last results have indicated that the yearly-$DRE_a$ was not very sensitive to the site location over Central Mediterranean land sites.

The annual cycle of the DRE by all (anthropogenic plus natural) and anthropogenic aerosols from measurements at Rome (Italy), a Central Mediterranean land site significantly affected by pollution, is investigated in this paper to further contribute to the

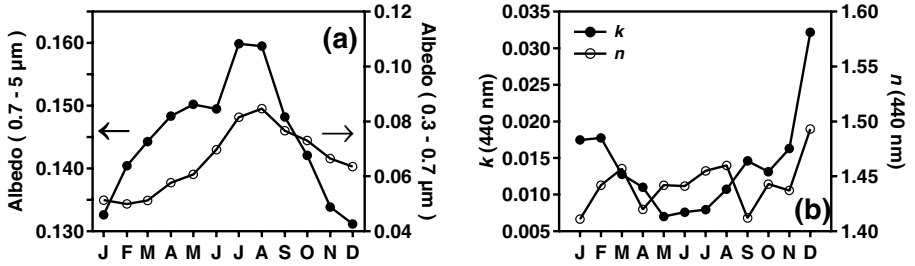


Fig. 1. – (a) Surface albedo monthly means based on MODIS MOD43B3 products for visibile (open dots) and near-infrared (full dots) wavelengths. (b) Monthly averaged real (open dots) and imaginary (full dots) refractive indices at 0.44 $\mu$m retrieved from Sun/sky photometer measurements.

characterization of the direct radiative forcing by aerosols over the Central Mediterranean. DRE and $DRE_a$ values are calculated by a two-stream radiative transfer model [7] at the ToA and at the surface: the ToA forcing is important to local and global radiation budgets, the sfc-forcing is important to surface heating and water evaporation [2]. Input data include monthly statistics of local aerosol column properties from AERONET Sun-sky photometer measurements and regional data on solar surface albedo from MODIS satellite sensor [8] for the year 2003. Clear- and all-sky conditions are investigated by adopting ISCCP monthly products for high-, mid-, and low-cloud cover [9].

A brief description of the two-stream radiative transfer code and input data is given in sect. **2**. Direct radiative forcing data are presented and discussed in sect. **3**. Summary and conclusion are in sect. **4**.

## 2. – Radiative transfer model and input data

The two-stream method [10] provides radiative fluxes at the boundary of homogeneous plane-parallel layers. Twenty homogeneous plane-parallel atmospheric layers are used in the two-stream model of this study to account for the changes with altitude of the atmospheric parameters and components. A detailed description of the model is given in [5, 7]. Daily-averaged radiative fluxes are determined for the solar (0.3–4 $\mu$m) and infrared (4–200 $\mu$m) spectral region. In order to account for the diurnal Sun elevation changes, solar radiative transfer simulations are performed at different Sun elevations and all available data are then properly weighted to get daily averaged solar radiative fluxes.

The standard, mid-latitude (30°–60° N), vertical profiles of density, pressure, temperature, and water vapour provided by the US Air Force Geophysics Laboratory (AFGL) for winter and summer are used in the model for meteorological parameters. Then, concentration vertical profiles of ozone, $N_2O$, $CO_2$, CO and $CH_4$ provided by AFGL, are used to account for absorption by atmospheric trace-gases.

**2˙1.** *Surface albedo.* – Surface albedo monthly means are based on "black-sky" albedo (directional-hemispherical reflectance) and "white-sky" albedo (bihemispherical reflectance) data from MODIS MOD43B3 products [11], which are provided every 16 days, at 1° × 1° resolution for three broad-bands: 0.3–0.7, 0.3–5.0, and 0.7–5.0 $\mu$m.

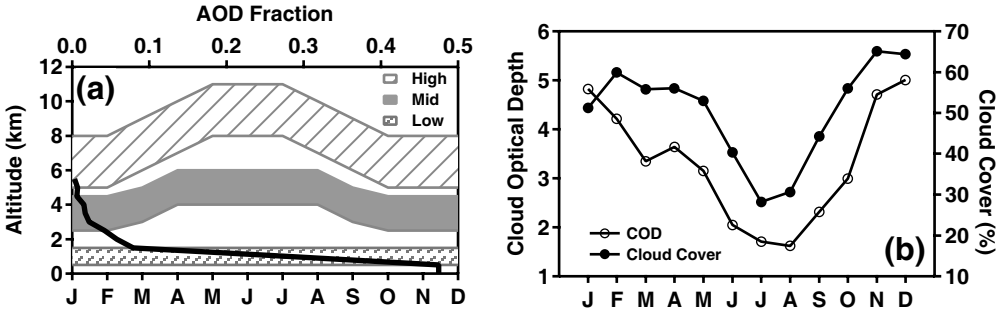


Fig. 2. – (a) Monthly evolution of the altitude location of high-, mid-, and low-level clouds (dashed areas) and vertical profile of the aerosol optical depth fraction (solid line). (b) Monthly evolution of cloud optical depth (COD, open dots) and cloud cover (full dots).

Figure 1a shows monthly averaged surface albedo values for the visible (0.3–0.7 $\mu$m) and infrared (0.7–5.0 $\mu$m) spectral range, respectively, retrieved from the 2003-year MOD43B3 products and for $1° \times 1°$ cell centred at 42.5° N, 12.5° E. A surface emissivity of 0.96 (and an albedo of 4%) is assumed in the far-infrared.

**2˙2.** *Cloud cover*. – Necessary cloud properties are based on the ISCCP D2 statistics [9], which supplies data defined by a multi-annual average (1984–2004) of monthly means of cloud scene optical depth for high-, mid-, and low-cloud cover. Figure 2 shows as a function of the months of the year (a) the altitude location of high-, mid-, and low-level clouds and (b) cloud optical depth (COD, open dots) and cloud cover (full dots) values used in the paper. Both COD and cloud cover values are quite dependent on seasons: spring-summer (SS, April-September) COD and cloud cover values are on average 57% and 72%, respectively, of the corresponding autumn-winter (AW, October-March) values. Hence, the interaction of the solar radiation with aerosol particles is favoured on SS over the Mediterranean basin.

**2˙3.** *AERONET aerosol properties for the* 2003 *year*. – The AERONET Sun/sky photometer is placed on the roof of the ISAC-CNR building (41.84° N; 12.65° E, 130 m asl) at Roma-Tor Vergata, in the southern suburbs of Rome, $\sim$ 15 km away from the city centre and $\sim$ 30 km away from the Tyrrhenian Sea. Rome is one of the largest Italian cities with more than 2.5 million of inhabitants and as a consequence it is quite affected by anthropogenic pollution.

Particle number size distributions and real ($n$) and imaginary ($k$) refractive indices from AERONET Sun/sky photometer measurements of the 2003 year, are used as input to the two-stream radiative transfer model to characterize aerosol properties. In particular, cloud-screened and quality-assured retrievals (level 2.0) from the Version 2 (V2) inversion algorithm are used. However, when level 2 AERONET products do not provide $n$ and $k$ values, the corresponding ones provided by level 1.5 AERONET products are used. A discussion on the accuracy of AERONET retrievals is reported in [12, 13] and it is also recalled in [7]. The numbers of measurements/month that have been properly weighted [7] to retrieve monthly aerosol optical and microphysical properties are given in table I where in brackets the number of measurement days/month also are reported.

Figure 3 shows the monthly averaged volume size distributions ($\mathrm{d}V(r)/\mathrm{dln}r$) retrieved from AERONET measurements during (a) autumn-winter and (b) spring-summer

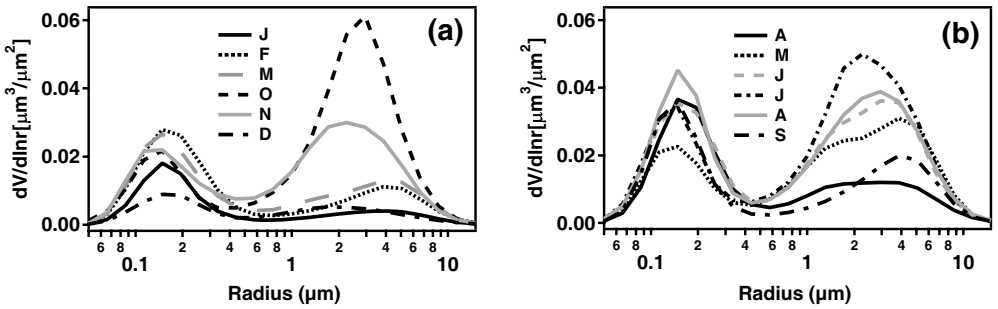


Fig. 3. – Monthly averaged volume size distributions retrieved from AERONET measurements during (a) autumn-winter and (b) spring-summer months of the 2003 year.

months of the 2003 year. The bimodal structure of fig. 3 spectra indicates that along with fine mode particles, which are mainly of anthropogenic origin, coarse-mode particles as those of natural (marine and crustal) origin, also contribute to the aerosol load all year along and mainly on SS.

AERONET real and imaginary refractive indices are retrieved at 0.44, 0.675, 0.87, and 1.02 $\mu$m, respectively. For the near-infrared region of the solar spectrum, refractive indices extracted for the wavelength at 1.02 $\mu$m are applied. For the far-infrared spectral region the refractive indices for tropospheric aerosol [14] are used. Figure 1b shows, as an example, monthly averaged real (open dots) and imaginary (full dots) refractive indices at 0.44 $\mu$m. We observe from fig. 1b that $n$ values span within the 1.4–1.5 range without

TABLE I. – *Monthly values of the factor f and number of AERONET measurements per month from which level* 2 *aerosol products are extracted. When level* 2 *AERONET products do not provide n and k values, the corresponding ones provided by level* 1.5 *AERONET products are used. The number of measurement days/month is given in brackets. Total measurements are also given.*

| | Number of measurements | $f$-values |
|---|---|---|
| January | 20(6) | 0.85 |
| February | 36(15) | 0.90 |
| March | 41(18) | 0.84 |
| April | 31(12) | 0.81 |
| May | 48(13) | 0.78 |
| June | 72(22) | 0.66 |
| July | 99(26) | 0.75 |
| August | 106(27) | 0.75 |
| September | 89(19) | 0.84 |
| October | 28(10) | 0.77 |
| November | 34(9) | 0.79 |
| December | 2(2) | 0.72 |
| Total | 606(179) | |

TABLE II. – *Basic statistics of the aerosol optical depth by all (*AOD*), fine (*$\mathrm{AOD_f}$*), and anthropogenic (*$\mathrm{AOD_a}$*) particles, of the single scattering albedo by all (SSA), fine (*$\mathrm{SSA_f}$*), and anthropogenic (*$\mathrm{SSA_a}$*) particles, and of the asymmetry factor by all (g), fine (*$g_\mathrm{f}$*), and anthropogenic (*$g_\mathrm{a}$*) particles. Mean values and standard deviations are based on monthly values. April-September and October-March monthly values are used to calculate Mean SS and Mean AW values, respectively and corresponding standard deviations.*

| | AOD | $\mathrm{AOD_f}$ | $\mathrm{AOD_a}$ |
|---|---|---|---|
| Mean | $(0.19 \pm 0.07)$ | $(0.15 \pm 0.05)$ | $(0.12 \pm 0.04)$ |
| Min–Max | 0.078–0.31 | 0.065–0.25 | 0.05–0.19 |
| Mean SS | $(0.24 \pm 0.06)$ | $(0.19 \pm 0.04)$ | $(0.14 \pm 0.03)$ |
| Mean AW | $(0.15 \pm 0.05)$ | $(0.12 \pm 0.04)$ | $(0.10 \pm 0.04)$ |
| | SSA | $\mathrm{SSA_f}$ | $\mathrm{SSA_a}$ |
| Mean | $(0.89 \pm 0.04)$ | $(0.92 \pm 0.04)$ | $(0.93 \pm 0.04)$ |
| Min–Max | 0.79–0.92 | 0.81–0.96 | 0.81–0.97 |
| Mean SS | $(0.91 \pm 0.01)$ | $(0.95 \pm 0.02)$ | $(0.95 \pm 0.02)$ |
| Mean AW | $(0.87 \pm 0.04)$ | $(0.90 \pm 0.05)$ | $(0.90 \pm 0.05)$ |
| | $g$ | $g_\mathrm{f}$ | $g_\mathrm{a}$ |
| Mean | $(0.66 \pm 0.01)$ | $(0.63 \pm 0.02)$ | $(0.63 \pm 0.02)$ |
| Min–Max | 0.64–0.68 | 0.60–0.65 | 0.60–0.65 |
| Mean SS | $(0.65 \pm 0.01)$ | $(0.62 \pm 0.02)$ | $(0.62 \pm 0.02)$ |
| Mean AW | $(0.66 \pm 0.01)$ | $(0.64 \pm 0.01)$ | $(0.64 \pm 0.01)$ |

any marked seasonal dependence. Conversely, $k$ values are quite dependent on seasons, they span within the 0.013–0.032 and 0.007–0.015 range on AW and SS, respectively. However, it worth mentioning that the rather high $k$ value of December is based on two measurement days (table I). In conclusion, fig. 1b and fig. 3 indicate that contributions of large-size, less-absorbing aerosols are larger on SS over the monitoring site. These results may partially be due to both the lack of rainy days, which favour the accumulation of natural and anthropogenic aerosols in the atmosphere and to the advection of large-size desert particles: Sahara dust outbreaks are more frequent on SS over the Mediterranean basin.

MIE calculations (assuming a spherical particle shape) are applied to translate the data on size, concentration and refractive indices into AODs (a measure of the magnitude of the aerosol extinction due to scattering and absorption), single scattering albedo (SSA) values (a measure of the relative importance of absorption and scattering), and asymmetry factors (a measure of the angular distribution of the scattering radiation). AOD, SSA, and asymmetry factor ($g$) represent the main parameters generally used to understand the complex interaction of aerosols with radiation. Figures 4a-c (full black symbols) show the time evolution of AOD, SSA, and $g$ monthly means at 0.55 $\mu$m, respectively recomputed from AERONET-derived aerosol size distributions and refractive indices. We observe from fig. 4a-c (full black symbols) that the mean columnar aerosol properties are quite dependent on seasons: particles of smaller SSA ($\mathrm{SSA} = 0.87 \pm 0.04$) and AOD ($\mathrm{AOD} = 0.15 \pm 0.05$) characterize the aerosol load on AW. SSA and AOD mean values $\pm 1$ std. dev. are $0.91 \pm 0.01$ and $0.24 \pm 0.06$, respectively, on SS. $g$-mean values are less dependent on seasons (table II). The comparison of fig. 4a-c (full black symbols) with the corresponding data of Oristano (39.91° N, 8.5° E) and Lecce (40.33° N, 18.10° E)

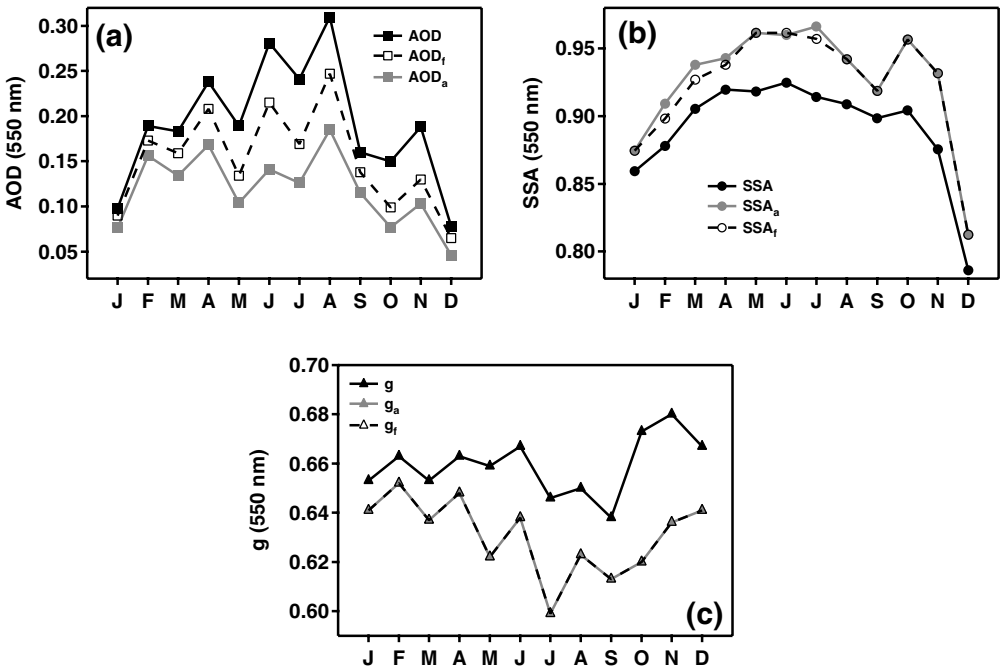


Fig. 4. – Monthly averaged (a) aerosol optical depths of all aerosols (AOD) and of the fine ($AOD_f$) and the anthropogenic ($AOD_a$) component.

reported in [5], reveals that Rome aerosol properties are rather close to the ones observed at Oristano and Lecce for the year 2003. In fact, it has been shown in [5] that aerosol properties are quite affected by latitude at land sites of the Central Mediterranean basin.

In accordance with the discussion reported in [5], the anthropogenic aerosol contribution is associated with a fraction of the sub-micron size particles. Potential anthropogenic contributions to the coarse size mode are ignored. Hence, the AERONET volume particle size distribution referring to particles with radius $0.05\,\mu\text{m} \leq r < 0.5\,\mu\text{m}$ is first used to calculate the number concentration of fine-mode aerosols $N_\text{f}(r)$. Then, only a fraction $f$ of $N_\text{f}(r)$ is considered of anthropogenic origin in accordance with the following relationship:

$$N_\text{a}(r) = f \cdot N_\text{f}(r), \tag{1}$$

where $N_\text{a}(r)$ is the number concentration of anthropogenic-only submicron aerosol particles. Monthly $f$-values that are given in table I are considered constant with particle size in the submicron fraction. $f$-values are based on LMDzT3.3 [15] global model-simulations [16]. In particular, inventories for global emissions of aerosols and pre-cursor gases for the years 2000 (current conditions) and 1750 (pre-industrial conditions) [17, 18] were used in the General Circulation Model LMDzT3.3 to calculate worldwide $f$-values.

MIE calculations are also applied to translate the data on number concentrations of fine ($N_\text{f}(r)$) and anthropogenic ($N_\text{a}(r)$) aerosols into aerosol optical depth, single-scattering albedo, and asymmetry factor of fine and anthropogenic particles, respectively. Refractive indices are not considered dependent on particle size. Figures 4a-c

show the time evolution of aerosol-optical-depth, single-scattering-albedo, and asymmetry factor monthly means of fine-mode ($AOD_f$, $SSA_f$, and $g_f$) and anthropogenic ($AOD_a$, $SSA_a$, and $g_a$) particles by open-black and full-grey symbols, respectively. Basic statistics of AOD, SSA, and $g$ values for all, fine, and anthropogenic particles are given in table II. Figure 4 shows that $AOD_a$ values are less dependent on seasons than AOD values. The $AOD_a$/AOD ratio that varies within the (0.51–0.83) range on AW, varies within the (0.50–0.71) range on SS as a consequence of the larger contribution of natural particles on SS. Conversely, $g_a$ values are on average 96% of $g$ values both on AW and SS. $SSA_a$ values are slightly larger than SSA values since refractive indices are not considered dependent on particle size.

**2˙4.** *Aerosol vertical distribution.* – The vertical profile of the aerosol optical depth fraction that is assumed constant all year along, is plotted in fig. 2a (solid line). It is equal to the one used in [5]. The lowermost 2 km layer contributes by $\sim 90\%$ to the total AOD.

## 3. – Aerosol direct radiative effects

The aerosol direct radiative effect (DRE) is defined as a change in a given radiative flux due to aerosols and the term "direct" refers to the interaction of aerosols with solar radiation and excludes the radiative influences of aerosols within clouds ("indirect effects"). Of particular interest for climate change over the industrial period are the top-of-atmosphere (ToA) and surface (sfc) DREs, defined here as the changes in the respective net fluxes due to scattering and absorption of shortwave (solar, 0.3–4 $\mu$m) and long wave (infrared, 4–200 $\mu$m) radiation by aerosols. Direct radiative effects by all (anthropogenic plus natural) and anthropogenic aerosols are calculated in this study to better infer the role of anthropogenic particles. DREs are calculated at the ToA and surface and within the atmosphere. The atmospheric forcing (AF) that is defined as the difference between ToA and surface aerosol DRE is and indicator of aerosol effects on atmosphere dynamics. The aerosol forcing efficiency (AFE, aerosol DRE per unit of AOD) that is mainly dependent on aerosol size and composition is also calculated. Finally, clear- and all-sky conditions are investigated by adopting ISCCP monthly products. To this end, it is worth recalling that AERONET measurements are essentially clear-sky and that it is assumed in this work that the average aerosol properties derived from AERONET can be extrapolated to all-sky conditions.

**3˙1.** *Aerosol DREs at solar wavelengths (*0.3–4 $\mu$m*).* – Figure 5a (full symbols) shows the monthly evolution of the all-sky (cld) ToA-DRE by total and anthropogenic particles at solar wavelengths: $(DRE_t^{cld})_{ToA}$ and $(DRE_a^{cld})_{ToA}$, respectively. Clear-sky (clr) ToA-DRE monthly means by total and anthropogenic particles, $(DRE_t^{clr})_{ToA}$ and $(DRE_a^{clr})_{ToA}$, respectively, are represented by open symbols. Figure 5b shows by full and open symbols the corresponding solar aerosol DRE at the surface at all sky ($(DRE_t^{cld})_{sfc}$ and $(DRE_a^{cld})_{sfc}$) and clear sky ($(DRE_t^{clr})_{sfc}$ and $(DRE_a^{clr})_{sfc}$), respectively. Basic statistics of all tested DRE parameters for all and anthropogenic particles are given in table III.

ToA- and sfc-$DRE_a$ monthly means are negative all year along with the exception of December $(DRE_t^{cld})_{ToA}$ and $(DRE_a^{cld})_{ToA}$ values, which are equal to 0.4 and 0.1 W/m$^2$, respectively for the larger presence of absorbing aerosols. Total and anthropogenic SSA values are 0.79 and 0.81, respectively on December. In contrast to greenhouse gases, which only cause warming, atmospheric aerosols, depending on their properties can cause

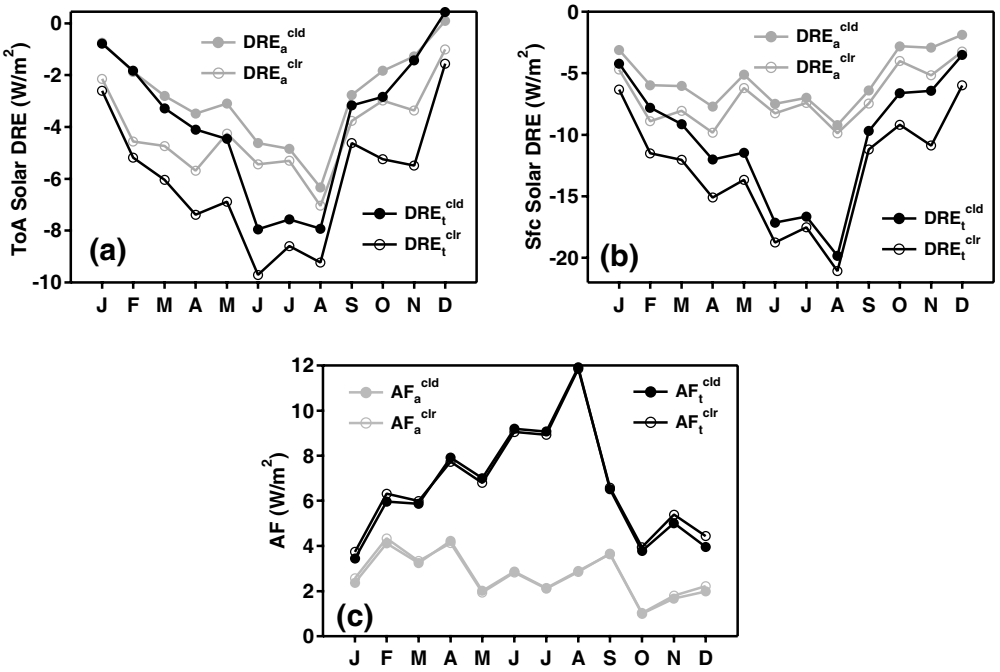


Fig. 5. – Monthly evolution in 2003 of the solar (0.3–4 $\mu$m) (a) ToA-DRE and (b) sfc-DRE by all aerosols (black symbols) and anthropogenic particles (grey symbols), at clear sky (open symbols) and all sky (full symbols).

either cooling or warming of the atmosphere. However, cloud covers and CODs also affect aerosol radiative effects. In fact, December $(DRE_{\rm t}^{\rm clr})_{\rm ToA}$ and $(DRE_{\rm a}^{\rm clr})_{\rm ToA}$ values are negative for the larger sunlight availability at clear-sky conditions, which favours scattering processes by atmospheric particles. Clouds reflect solar radiation back to space and reduce sunlight available for aerosol interactions, as a consequence, solar aerosol DREs reduce in magnitude at all sky. The percentage reduction with respect to the clear-sky aerosol DRE is larger in winter than in summer in part because there is less cloud cover and cloud optical depth during summer (fig. 2). Figure 5a reveals that at the ToA, the DRE absolute mean percentage reduction is of 62% and 26% on AW and SS, respectively for the total aerosol component, while it is of 50% and 21% on AW and SS, respectively for anthropogenic particles. At the surface (fig. 5b), the DRE absolute mean percentage reduction is of 34% and 12% on AW and SS, respectively, for both all and anthropogenic aerosols.

Negative ToA and surface DRE values indicate a cooling of the Earth-Atmosphere-System by aerosols, as extra solar radiation is reflected back to space. Figure 5 shows that aerosol associated reductions of the downward solar radiation at the Earth's surface are larger, as aerosols not only scatter but also absorb solar radiation. In fact, the comparison of fig. 5a and fig. 5b allows inferring that sfc-DRE monthly means by all aerosols are on average more than twice larger than the corresponding ToA-DRE monthly means at clear-sky: $(DRE_{\rm t}^{\rm clr})_{\rm sfc}/(DRE_{\rm t}^{\rm clr})_{\rm ToA}$ ratios span within the (1.9–3.9) and (1.9–2.4) range on AW and SS, respectively. The anthropogenic-aerosol associated reduction of the downward solar radiation at the Earth's surface is slightly smaller than that due to all aerosols:

TABLE III. – *Basic statistics (mean value ±1 std. dev and minimum and maximum values and spring-summer and autumn-winter mean values ±1 std. dev.) of the parameters used to evaluate the solar DRE by all and anthropogenic particles at clear and all sky.*

| (W m$^{-2}$) | $(DRE_{\mathrm{t}}^{\mathrm{clr}})_{\mathrm{ToA}}$ | $(DRE_{\mathrm{a}}^{\mathrm{clr}})_{\mathrm{ToA}}$ | $(DRE_{\mathrm{t}}^{\mathrm{cld}})_{\mathrm{ToA}}$ | $(DRE_{\mathrm{a}}^{\mathrm{cld}})_{\mathrm{ToA}}$ |
|---|---|---|---|---|
| Mean | $-(6.0 \pm 2.5)$ | $-(4.2 \pm 1.7)$ | $-(3.7 \pm 2.8)$ | $-(2.8 \pm 1.8)$ |
| Min; Max | $-(9.7; 1.6)$ | $-(7.0; 1.0)$ | $-7.9; 0.4$ | $-6.3; 0.1$ |
| Mean SS | $-(7.7 \pm 1.8)$ | $-(5.3 \pm 1.1)$ | $-(5.8 \pm 2.1)$ | $-(4.2 \pm 1.3)$ |
| Mean AW | $-(4.4 \pm 1.8)$ | $-(3.1 \pm 1.4)$ | $-(1.6 \pm 1.3)$ | $-(1.4 \pm 1.0)$ |
| (W m$^{-2}$) | $(DRE_{\mathrm{t}}^{\mathrm{clr}})_{\mathrm{sfc}}$ | $(DRE_{\mathrm{a}}^{\mathrm{clr}})_{\mathrm{sfc}}$ | $(DRE_{\mathrm{t}}^{\mathrm{cld}})_{\mathrm{sfc}}$ | $(DRE_{\mathrm{a}}^{\mathrm{cld}})_{\mathrm{sfc}}$ |
| Mean | $-(12.8 \pm 4.6)$ | $-(6.9 \pm 2.2)$ | $-(10.4 \pm 5.2)$ | $-(5.5 \pm 2.3)$ |
| Min; Max | $-(21.1; 11.2)$ | $-(9.9; 3.2)$ | $-(19.8; 9.7)$ | $-(9.2; 1.9)$ |
| Mean SS | $-(16.2 \pm 3.6)$ | $-(8.2 \pm 1.4)$ | $-(14.5 \pm 3.9)$ | $-(7.2 \pm 1.8)$ |
| Mean AW | $-(9.3 \pm 2.6)$ | $-(5.6 \pm 2.2)$ | $-(6.3 \pm 2.1)$ | $-(3.8 \pm 1.4)$ |
| (W m$^{-2}$) | $AF_{\mathrm{t}}^{\mathrm{clr}}$ | $AF_{\mathrm{a}}^{\mathrm{clr}}$ | $AF_{\mathrm{t}}^{\mathrm{cld}}$ | $AF_{\mathrm{a}}^{\mathrm{cld}}$ |
| Mean | $6.8 \pm 2.4$ | $2.7 \pm 1.0$ | $6.7 \pm 2.5$ | $2.7 \pm 1.1$ |
| Min; Max | 3.7; 11.8 | 1.0; 4.3 | 3.4; 11.9 | 1; 4.2 |
| Mean SS | $8.5 \pm 1.9$ | $2.9 \pm 0.9$ | $8.7 \pm 1.9$ | $3.0 \pm 0.9$ |
| Mean AW | $4.9 \pm 1.1$ | $2.5 \pm 1.2$ | $4.7 \pm 1.1$ | $2.4 \pm 1.1$ |
| (W m$^{-2}$) | $(AFE_{\mathrm{t}}^{\mathrm{clr}})_{\mathrm{ToA}}$ | $(AFE_{\mathrm{a}}^{\mathrm{clr}})_{\mathrm{ToA}}$ | $(AFE_{\mathrm{t}}^{\mathrm{cld}})_{\mathrm{ToA}}$ | $(AFE_{\mathrm{a}}^{\mathrm{cld}})_{\mathrm{ToA}}$ |
| Mean | $-(30.6 \pm 4.7)$ | $-(34.3 \pm 5.9)$ | $-(16.9 \pm 10.4)$ | $-(21.4 \pm 11.8)$ |
| Min-Max | $-(36.4; 19.9)$ | $-(42.1; 21.9)$ | $-31.4; 5.7$ | $-38.5; 2.1$ |
| Mean SS | $-(32.7 \pm 3.2)$ | $-(37.7 \pm 3.7)$ | $-(24.3 \pm 5.2)$ | $-(30.0 \pm 6.6)$ |
| Mean AW | $-(28.5 \pm 5.4)$ | $-(31.0 \pm 6.0)$ | $-(9.4 \pm 8.9)$ | $-(12.8 \pm 9.2)$ |
| (W m$^{-2}$) | $(AFE_{\mathrm{t}}^{\mathrm{clr}})_{\mathrm{sfc}}$ | $(AFE_{\mathrm{a}}^{\mathrm{clr}})_{\mathrm{sfc}}$ | $(AFE_{\mathrm{t}}^{\mathrm{cld}})_{\mathrm{sfc}}$ | $(AFE_{\mathrm{a}}^{\mathrm{cld}})_{\mathrm{sfc}}$ |
| Mean | $-(66.7 \pm 5.5)$ | $-(58.7 \pm 5.2)$ | $-(51.9 \pm 10.7)$ | $-(45.0 \pm 8.2)$ |
| Min; Max | $-(76.7; 57.9)$ | $-(69.6; 50.4)$ | $-(68.9; 34.26)$ | $-(55.7; 28.6)$ |
| Mean SS | $-(68.8 \pm 3.5)$ | $-(58.9 \pm 3.6)$ | $-(60.9 \pm 6.0)$ | $-(51.5 \pm 3.9)$ |
| Mean AW | $-(64.5 \pm 6.6)$ | $-(58.6 \pm 6.9)$ | $-(43.0 \pm 5.2)$ | $-(38.4 \pm 5.6)$ |

$(DRE_{\mathrm{a}}^{\mathrm{clr}})_{\mathrm{sfc}}/(DRE_{\mathrm{a}}^{\mathrm{clr}})_{\mathrm{ToA}}$ ratios span within the (1.3–3.2) and (1.4–2.0) range on AW and SS, respectively. It is worth observing (fig. 5a) both that the seasonal evolution of the anthropogenic particle's DRE is similar to that one due to all aerosols at the ToA and that the ToA-DRE is mostly due to anthropogenic particles: on average 70% and 75% of the ToA-DRE by all aerosols is due to anthropogenic particles at clear and all sky, respectively. The role of the anthropogenic particle's DRE is smaller at the surface (fig. 5b). On average 55% of the surface DRE by all aerosols is due to anthropogenic particles both at clear and all sky. In particular, the mean sfc-DRE ±1 std. dev. by anthropogenic particles is $-(5.6 \pm 2.2)\,\mathrm{W/m^2}$ and $-(8.2 \pm 1.4)\,\mathrm{W/m^2}$ on AW and SS, respectively at clear sky. While, at all-sky mean $(DRE_{\mathrm{a}}^{\mathrm{cld}})_{\mathrm{sfc}}$ values are $-(3.8 \pm 1.8)\,\mathrm{W/m^2}$ and $-(7.2 \pm 1.4)\,\mathrm{W/m^2}$ on AW and SS, respectively. Atmospheric-forcing monthly means (fig. 5c) allow inferring that the anthropogenic particle's effects on atmospheric dynamics are poorly dependent on seasons ($\mathrm{AF_a}$ mean values are $3.0 \pm 0.9\,\mathrm{W/m^2}$ and $2.4 \pm 1.1\,\mathrm{W/m^2}$ on SS and AW, respectively) despite the ones by all aerosols. As a consequence, the mean atmospheric

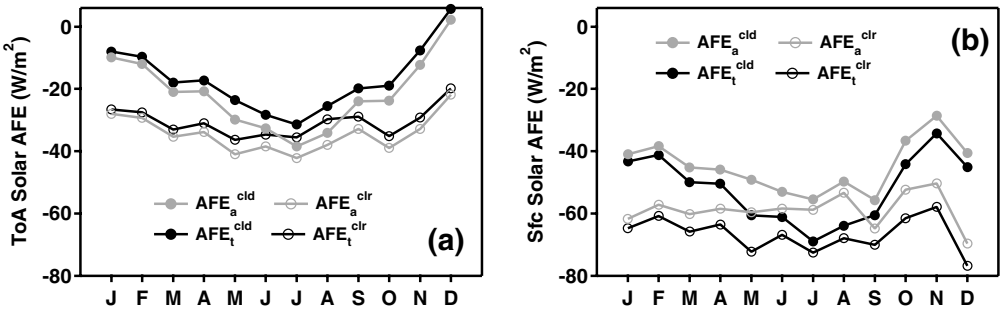


Fig. 6. – Monthly evolution in 2003 of the solar (0.3–4 $\mu$m) (a) ToA-AFE and (b) sfc-AFE by all aerosols (black symbols) and anthropogenic particles (grey symbols), at clear sky (open symbols) and all sky (full symbols).

forcing by anthropogenic particles is 50% and 36% of the AF by all aerosols on AW and SS, respectively (table III), both at clear and all sky. These last results are mainly due to the smaller dependence on seasons of the aerosol optical depth by anthropogenic particles.

Monthly means of clear- and all-sky aerosol forcing efficiencies referring to 550 nm aerosol-optical-depths by all and anthropogenic aerosols are plotted in figs. 6a,b. We observe from fig. 6 that forcing-efficiency's monthly means of both the all-aerosols (black-open symbols) and the anthropogenic particles (grey-open symbols) are poorly affected by seasons at clear sky. This result indicates that the seasonal trend of the DRE observed both at the ToA and at the surface is mainly affected by the seasonal dependence of the AOD and less by the dependence on seasons of aerosol optical and microphysical properties: AFEs are mainly dependent on aerosol size and composition as mentioned. To this end it is worth noting that the marked dependence on seasons that characterize all-sky aerosol forcing efficiencies (full symbols) is mainly determined by the variations with seasons of cloud covers and cloud optical depths. Table III data facilitate the comparison between DREs by all and anthropogenic aerosols both at clear and all sky. In addition, the comparison of the all-sky data by anthropogenic particles of table III with the corresponding ones of [5] referring to Oristano and Lecce reveals that the differences between mean values of all tested parameters are smaller than associated standard deviations, even if Oristano and Lecce are less affected by pollution than Rome. The significant dependence of aerosol properties on latitude over land sites of the Central Mediterranean [5] is responsible for these last results. It is also worth mentioning that yearly mean values of $(DRE_{\rm a}^{\rm cld})_{\rm ToA}$, $(DRE_{\rm a}^{\rm cld})_{\rm sfc}$, $(AFE_{\rm a}^{\rm cld})_{\rm ToA}$, $(AFE_{\rm a}^{\rm cld})_{\rm sfc}$, and $AF_{\rm a}^{\rm cld}$ are quite similar to the corresponding yearly mean values reported in [5] for Central Mediterranean land sites, even if monthly mean values vary from site to site. Hence, these last results further more indicate that the yearly DRE by anthropogenic particles is not very sensitive to the site location over Central Mediterranean land sites, in accordance with [5].

**3**˙2. *Aerosol DREs at infrared wavelengths (*4–200 $\mu$m*).* – The infrared (IR) ToA-DRE (also often referred to as greenhouse effect, as thermal energy is retained in the Earth-Atmosphere-System) requires significant IR aerosol optical depth (*e.g.*, coarse size aerosols). Indeed, a significant IR ToA effect by tropospheric aerosols is only expected

TABLE IV. – *Basic statistics of the clear- and all-sky infrared DRE by all and anthropogenic aerosols at the surface and at the ToA.*

| (W m$^{-2}$) | $(DRE_{\mathrm{t}}^{\mathrm{clr}})_{\mathrm{ToA}}$ | $(DRE_{\mathrm{a}}^{\mathrm{clr}})_{\mathrm{ToA}}$ | $(DRE_{\mathrm{t}}^{\mathrm{cld}})_{\mathrm{ToA}}$ | $(DRE_{\mathrm{a}}^{\mathrm{cld}})_{\mathrm{ToA}}$ |
|---|---|---|---|---|
| Mean | $0.54 \pm 0.31$ | $0.05 \pm 0.02$ | $0.36 \pm 0.25$ | $0.02 \pm 0.02$ |
| Min; Max | 0.11; 0.98 | 0.01; 0.09 | 0.06; 0.81 | 0.00; 0.05 |
| Mean SS | $0.75 \pm 0.20$ | $0.06 \pm 0.02$ | $0.53 \pm 0.22$ | $0.04 \pm 0.01$ |
| Mean AW | $0.34 \pm 0.26$ | $0.03 \pm 0.01$ | $0.17 \pm 0.14$ | $0.007 \pm 0.005$ |
| (W m$^{-2}$) | $(DRE_{\mathrm{t}}^{\mathrm{clr}})_{\mathrm{sfc}}$ | $(DRE_{\mathrm{a}}^{\mathrm{clr}})_{\mathrm{sfc}}$ | $(DRE_{\mathrm{t}}^{\mathrm{cld}})_{\mathrm{sfc}}$ | $(DRE_{\mathrm{a}}^{\mathrm{cld}})_{\mathrm{sfc}}$ |
| Mean | $1.32 \pm 0.59$ | $0.26 \pm 0.08$ | $0.86 \pm 0.53$ | $0.16 \pm 0.07$ |
| Min; Max | 0.41; 2.11 | 0.09; 0.36 | 0.18; 1.77 | 0.04; 0.29 |
| Mean SS | $1.61 \pm 0.49$ | $0.29 \pm 0.05$ | $1.20 \pm 0.50$ | $0.21 \pm 0.05$ |
| Mean AW | $1.03 \pm 0.57$ | $0.23 \pm 0.09$ | $0.52 \pm 0.30$ | $0.12 \pm 0.05$ |

from elevated dust layers over cloud-free scenes and warm surfaces. The IR surface DRE requires IR opacity (*e.g.*, coarse size aerosol) at temperatures not too much below that of the surface. Thus, largest IR surface effects are expected from coarse (sea-salt and dust) aerosols near the surface. However, the IR effect of tropospheric aerosols and in particular of anthropogenic aerosols (being $< 1\,\mu$m in maximum dimension) is often neglected, because IR-DREs are small compared to the solar effects, especially at the ToA.

Basic statistics of ToA and surface IR-DREs by all and anthropogenic aerosols are given in table IV. ToA and surface DREs are always positive. Hence, aerosols produce planetary and surface warming through interaction with IR radiation. Clear-sky IR-DREs by all aerosols vary within the 0.4–2.1 W/m$^2$ and 0.1–1.0 W/m$^2$ range at the surface and at the ToA, respectively. While, clear-sky IR-DREs by anthropogenic aerosols vary within the 0.1–0.4 W/m$^2$ range at the surface and are lower than 0.1 W/m$^2$ at the ToA. Clouds, due to their own greenhouse effect, reduce the IR aerosol DRE both at the ToA and at the surface. Percentage reductions with respect to the clear-sky IR-DREs by anthropogenic aerosols are of about 40% and 60% at the surface and ToA, respectively.

## 4. – Conclusions

All- and clear-sky DREs by all (anthropogenic plus natural) and anthropogenic aerosols have been calculated for the year 2003 to address the anthropogenic aerosol's impact at a polluted land site (Rome, Italy) of the Central Mediterranean. The analysis of aerosol optical and microphysical properties has revealed that the contribution of large-size, less-absorbing aerosols, which are expected to be of natural origin, gets quite large on SS over the monitoring site. As a consequence, the $\mathrm{AOD_a/AOD}$ ratio at 550 nm that varies within the (0.51–0.83) range on AW, varies within the (0.50–0.71) range on SS. Mean $\mathrm{AOD_a}$ values $\pm 1$ std. dev. at 550 nm are: $0.14 \pm 0.03$ and $0.10 \pm 0.04$ on AW and SS, respectively. $g_{\mathrm{a}}$ values are on average 96% of $g$ values both on AW and SS.

The aerosol DRE analysis has revealed that ToA-DRE values are more affected by anthropogenic particles. In fact, on average 70% and 75% of the ToA-DRE by all aerosols is due to anthropogenic particles at clear and all sky, respectively. Conversely, the surface DRE by anthropogenic particles is on average 55% of the one by all aerosols both at clear and all sky.

Atmospheric-forcing monthly means that are positive all year round since aerosol associated reductions of the downward solar radiation at the Earth's surface are larger, have revealed that anthropogenic particles are on average responsible of 50% and 36% of the AF by all aerosols on AW and SS, respectively, both at clear and all sky. Anthropogenic particle's effects on atmospheric dynamics are poorly dependent on seasons: $AF_a$ mean values are $3.0 \pm 0.9\,W/m^2$ and $2.4 \pm 1.1\,W/m^2$ on SS and AW, respectively despite AF values. Aerosol forcing efficiencies that are poorly affected by seasons at clear sky have allowed inferring that the seasonal trend of ToA- and sfc-DREs by all and anthropogenic particles is mainly affected by the seasonal dependence of aerosol optical depths and less by the aerosol optical and microphysical property changes with the time of the year. COD and cloud cover effects on the seasonality of all tested parameters have also been highlighted. Finally, the comparison of $(DRE_a^{cld})_{ToA}$, $(DRE_a^{cld})_{sfc}$, $(AFE_a^{cld})_{ToA}$, $(AFE_a^{cld})_{sfc}$, and $AF_a^{cld}$ yearly mean values with the corresponding ones reported in [5] for Central Mediterranean land sites has further more revealed that the yearly DRE by anthropogenic particles is not very sensitive to the site location over Central Mediterranean land sites, even if monthly values can significantly vary from site to site. The negligible role of DREs by anthropogenic particles at infrared wavelengths has also been demonstrated.

In conclusion this paper that highlights role and main characteristics of DREs by anthropogenic particles at a site (Rome, Italy) significantly affected by pollution for the year 2003, also contributes to the characterization of aerosol DREs by all and anthropogenic aerosols over the Mediterranean basin: an area quite sensitive to climate change. Work is in progress to investigate the year by year variability of aerosol DREs over the Mediterranean basin.

* * *

We greatly acknowledge Dr. S. Kinne for providing the radiative transfer model. This work has been supported by *Ministero dell' Istruzione dell'Università e della Ricerca* of Italy (Programma di Ricerca 2006. Prot. 2006027825), by the European Project EARLINET-ASOS (2006 -2011, Contract n. 025991), by Progetto FISR AEROCLOUDS and by Centro Euro Mediterraneo per i Cambiamenti Climatici (CMCC). The authors kindly acknowledge the Principal Investigator of the AERONET station of Roma-Tor Vergata.

REFERENCES

[1] Intergovernmental Panel on Climate Change (IPCC): *Climate change 2007, The Physical Science Basis – Summary for Policymakers*, `http://ipccwg1.ucar.edu/wg1/wg1_home.html`. (2007).

[2] Bates T. S., Anderson T. L., Baynard T., Bond T., Boucher O., Carmichael G., Clarke A., Erlick C., Guo H., Horowitz L., Howell S., Kulkarni S., Maring H., MC Comiskey A., Middlebrook A., Noone K., O'Dowd C. D., Ogren J., Penner J., Quinn P. K., Ravishankara A. R., Savoie D. L., Schwartz S. E., Shinozuka Y., Tang Y., Weber R. J. and Wu Y., *Atmos. Chem. Phys.*, **6** (2006) 1657.

[3] Giorgi F., *J. Geophys. Res.*, **33** (2006) L08707, doi:10.1029/2006GL025734.

[4] Chung C. E., Ramanathan V., Kim D. and Podgorny I. A., *J. Geophys. Res.*, **110** (2005) D24207, doi:10.1029/2005JD006356.

[5] Bergamo A., Tafuro A. M., Kinne S., De Tomasi F. and Perrone M. R., *Atmos. Chem. Phys.*, **8** (2008) 6995.

[6] Holben B. N., Eck T. F., Slutsker I., Tanré D., Buis J. P., Setzer A., Vermote E., Reagan J. A., Kaufman Y., Nakajima T., Lavenu F., Jankowiak I. and Smirnov A., *Remote Sens. Environ.*, **6** (1998) 1.
[7] Tafuro A. M., Kinne S., De Tomasi F. and Perrone M. R., *J. Geophys. Res.*, **112** (2007) D20202, doi:10.1029/2006JD008265.
[8] King M. D., Kaufman Y. J., Menzel W. P. and Tanré D., *IEEE Trans. Geosci. Remote Sensing*, **30** (1992) 1.
[9] Rossow W. B. and Schiffer R. A., *Bull. Am. Meteorol. Soc.*, **80** (1999) 2261.
[10] Meador W. E and Weaver W. R., *J. Atm. Sci.*, **37** (1980) 630.
[11] Schaaf C. B., Gao F., Strahler A. H., Lucht W., Li X., Tsang T., Strugnell N. C., Zhang X., Jin Y., Muller J.-P., Lewis P., Barnsley M., Hobson P., Disney M., Roberts G., Dunderdale M., Doll C., D'Entremont R. P., Hu B., Liang S., Privette J. L. and Roy D., *Remote Sens. Environ.*, **83** (2002) 135.
[12] Dubovik O., Smirnov A., Holben B. N., King M. D., Kaufman Y. J., Eck T. F. and Slutsker I., *J. Geophys. Res.*, **105 (D8)** (2000) 9791.
[13] Dubovik O., Holben B. N., Lapyonok T., Sinyuk A., Mishchenko M. I., Yang P. and Slutsker I., *Geophys. Res. Lett.*, **29 (10)** (2002) 54(1).
[14] Paltridge G. W. and Platt C. M. R., *Radiative Processes in Meteorology and Climatology* (Elsevier Publishing Com., Amsterdam) 1976, pp. 318+VII.
[15] Reddy M. S., Boucher O., Balanski Y. and Schulz M., *Geophys. Res. Lett.*, **32** (2005) L12803, doi:10.1029/2004GL021743.
[16] Schulz M., Textor C., Kinne S., Balkanski Y., Bauer S., Berntsen T., Berglen T., Boucher O., Dentener F., Guibert S., Isaksen I. S. A., Iversen T., Koch D., Kirkevag A., Liu X., Montanaro V., Myhre G., Penner J. E., Pitari G., Reddy S., Seland Ø., Stier P. and Takemura T., *Atmos. Chem. Phys.*, **6** (2006) 5225.
[17] Dentener F., Kinne S., Bond T., Boucher O., Cofala J., Generoso S., Ginoux P., Gong S., Hoelzemann J. J., Ito A., Marelli L., Penner J. E., Putaud J.-E., Textor C., Schulz M., Van Der Werf G. R. and Wilson J., *Atmos. Chem. Phys.*, **6** (2006) 4321.
[18] Steir P., Seinfeld J. H., Kinne S. and Boucher O., *Atmos. Chem. Phys.*, **7** (2007) 5237.